Environmental Science & Technology

pubs.acs.org/est

Article

Significance of Co-ion Partitioning in Salt Transport through Polyamide Reverse Osmosis Membranes

Li Wang, Tianchi Cao, Kevin E. Pataroque, Masashi Kaneda, P. Maarten Biesheuvel, and Menachem Elimelech*

Cite This: *Environ. Sci. Technol.* 2023, 57, 3930−3939

Read Online

ACCESS | Metrics & More | Article Recommendations | Supporting Information

ABSTRACT: Salt permeability of polyamide reverse osmosis (RO) membranes has been shown to increase with increasing feed salt concentration. The dependence of salt permeability on salt concentration has been attributed to the variation of salt partitioning with feed salt concentration. However, studies using various analytical techniques revealed that the salt (total ion) partitioning coefficient decreases with increasing salt concentration, in marked contrast to the observed increase in salt permeability. Herein, we thoroughly investigate the dependence of total ion and co-ion partitioning coefficients on salt concentration and solution pH. The salt partitioning is measured using a quartz crystal microbalance (QCM), while the co-ion partitioning is calculated from the measured salt partitioning using a modified Donnan theory. Our results demonstrate that the co-ion and total ion partitioning behave entirely differently with increasing salt concentrations. Specifically, the co-ion partitioning increased fourfold, while total ion partitioning decreased by 60% as the salt (NaCl) concentration increased from 100 to 800 mM. The increase in co-ion partitioning with increasing salt concentration is in accordance with the increasing trend of salt permeability in RO experiments. We further show that the dependence of salt and co-ion partitioning on salt concentration is much more pronounced at a higher solution pH. The good co-ion exclusion (GCE) model—derived from the solution−friction model—is used to calculate the salt permeability based on the co-ion partitioning coefficients. Our results show that the GCE model predicts the salt permeabilities in RO experiments relatively well, indicating that co-ion partitioning, not salt partitioning, governs salt transport through RO membranes. Our study provides an in-depth understanding of ion partitioning in polyamide RO membranes and its relationship with salt transport.

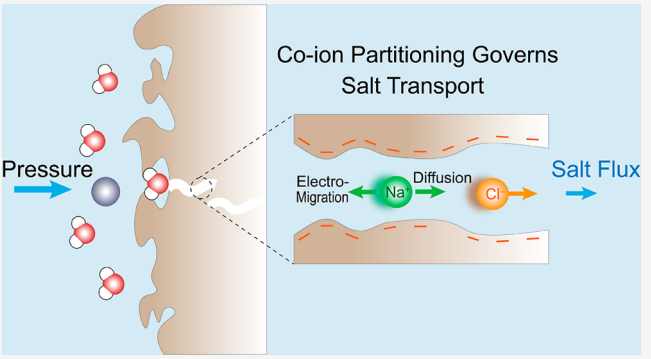

KEYWORDS: *reverse osmosis, salt transport, salt partitioning, co-ion partitioning, quartz crystal microbalance, solution−friction model*

INTRODUCTION

Reverse osmosis (RO) is the dominant technology for desalination and water purification due to its high energy efficiency and superior product water quality. In the RO process, hydraulic pressure is applied to the saline feed stream to drive water molecules across a semipermeable membrane while rejecting the salt ions. Thin-film composite (TFC) membranes are state-of-the-art RO membranes, with an aromatic polyamide (PA) active layer on top of a nonselective porous polysulfone support layer.[1] The thin (a few hundreds of nanometers), highly cross-linked active layer is formed by the interfacial polymerization of *m*-phenylenediamine (MPD) and trimesoyl chloride (TMC).[2]

Transport of salt and water through the PA active layer is critically important for RO desalination performance as it governs the water−salt selectivity of the TFC membranes. However, despite the wide use of RO technology, there is a lack of fundamental understanding of the mechanisms of salt and water transport in RO membranes. The phenomenological solution−diffusion (SD) model is commonly used to describe water and salt transport through the active layer of RO membranes.[1,3,4] The SD model assumes that the active layer is a nonporous polymer phase, with water and salt transport driven by the concentration gradient. Specifically, salt flux in the SD model is proportional to the salt concentration difference across the membrane, with a proportionality (or salt permeability) coefficient that is independent of operating conditions (i.e., feed salt concentration and permeate water flux).

Recent studies, however, have demonstrated that salt permeability in RO membranes significantly increases with

Received: December 27, 2022
Revised: February 9, 2023
Accepted: February 9, 2023
Published: February 23, 2023

increasing feed salt concentration.[5−7] Based on the SD model, the salt permeability is determined by the product of the salt partitioning coefficient and salt diffusion coefficient inside the membrane.[1,3,8] As the salt diffusion coefficient inside the membrane is relatively insensitive to salt concentration, the dependence of salt permeability on salt concentration has been ascribed to the dependence of the salt partitioning coefficient on salt concentration.[8,9]

Significant progress has been made in quantifying salt partitioning into the PA layer of TFC membranes by various analytical techniques, including quartz crystal microbalance (QCM),[10−12] electrochemical impedance spectroscopy,[13−15] and Rutherford backscattering spectroscopy.[16] However, all these studies demonstrated that the salt partitioning coefficient decreases with increasing salt concentrations, in contrast to the common experimental observations of increased salt permeability as the feed salt concentration increases. Hence, there is a crucial need for an in-depth investigation of salt partitioning in RO and its relationship with salt transport mechanisms and membrane salt permeability.

Given that the PA active layer of RO membranes is negatively charged due to unreacted carboxyl groups within the PA layer,[17−19] the partitioning of anions (i.e., co-ions) is different from that of cations (i.e., counter-ions). Specifically, the fixed negatively charged groups inside the PA membrane favor the partitioning of counter-ions and hinder the partitioning of co-ions. The overall salt flux, however, is controlled by the species with less permeability (i.e., co-ions).[20−23] Therefore, the behavior of co-ions is the limiting factor and thus governs the overall salt flux across the RO membranes. To date, however, no studies have been reported on quantifying the partitioning coefficient of co-ions and relating it to salt permeability in RO membranes.

In this study, we developed a method to quantify the partitioning coefficient of co-ions into the PA active layer of RO membranes based on the measured total ion (salt) partitioning using a QCM. We demonstrate starkly different behaviors of co-ion partitioning and total ion (salt) partitioning at different salt concentrations and solution pHs. Notably, our results reveal that co-ion partitioning increases as the feed salt concentration increases, in contrast to the total ion partitioning which continuously decreases with increasing salt concentration. Additionally, as the solution pH is increased, the partitioning coefficient of salt increases while that of co-ions decreases. The measured salt permeabilities of RO membranes were dependent on the co-ion partitioning coefficient, not the total ion (salt) partitioning coefficient, in agreement with the good co-ion exclusion (GCE) model. Our results highlight the significance of co-ion partitioning—not salt partitioning as implied by the SD model—in governing salt transport through RO membranes.

THEORY

Solution−Friction Model for Salt Flux in RO Membranes. Salt transport through RO membranes can be described by the solution−friction model.[5,24] The model is based on the generalized Maxwell−Stefan framework, which is obtained from a force balance on the individual species in the system. Specifically, the driving force for salt transport in RO membranes is the gradient of chemical potential, compensated by the frictional forces exerted on the salt ions. The frictional forces arise due to the difference in velocities between the ions and water as well as that between the ions and the membrane matrix.[5,24] These frictional forces can be expressed as the product of the velocity difference and the frictional coefficient between the species (i.e., ions and membrane and ions and water).

The force balance can be written as[25,26]

$$-\nabla\mu_i = \sum_j RTf_{i-j}(v_i - v_j) = RTf_{i-w}(v_i - v_w) + RTf_{i-m}(v_i - v_m) \quad (1)$$

where μ_i is the chemical potential of salt ions, f_{i-w} and f_{i-m} are the frictional coefficients between ions and water and between ions and the membrane, and v_i, v_w, and v_m are the velocities of ions, water, and the membrane, respectively. As the membrane is stationary, v_m is zero. In addition, the chemical potential (μ_i) is collectively contributed by the concentration and electrical potential

$$\mu_i = \mu_i^0 + RT \ln c_i + RTz_i\varphi \quad (2)$$

where μ_i^0 is the chemical potential at the reference state, R is the gas constant, T is the absolute temperature, c_i is the ion concentration inside the membrane, z_i is the ion valence, and φ is the dimensionless electrical potential. Substituting eq 2 in eq 1 and rearranging yields the ion velocity[5]

$$v_i = \frac{f_{i-w}}{f_{i-w} + f_{i-m}}v_w - \frac{1}{f_{i-w} + f_{i-m}}\left(\frac{\partial \ln c_i}{\partial x} + z_i\frac{\partial\varphi}{\partial x}\right) \quad (3)$$

The flux of ion i, a product of ion concentration and ion velocity, can be calculated as

$$J_i = K_{f,i}c_i v_w - K_{f,i}D_i\left(\frac{\partial c_i}{\partial x} + z_i c_i\frac{\partial\varphi}{\partial x}\right) \quad (4)$$

where J_i is the ion flux, $K_{f,i}$ is the frictional factor, and D_i is the diffusion coefficient of ion in the membrane. The latter can be approximated as the product of the ion diffusion coefficient in bulk solution and the effective porosity of the membrane.[27] By comparing eqs 3 and 4, we show that $K_{f,i}$ is related to the frictional coefficients via the following equation

$$K_{f,i} = \frac{f_{i-w}}{f_{i-w} + f_{i-m}} \quad (5)$$

In addition, D_i is proportional to the inverse of f_{i-w} as described by the Einstein relation[28]

$$D_i = \frac{RT}{f_{i-w}} \quad (6)$$

We note that eq 4 is identical to the ion flux described by the solution−friction (SF) model.[5,24]

Salt Permeability Based on the GCE Model. Due to the low Peclet number in RO membranes, the contribution of advection (first term on the right-hand side of eq 4) to the ion flux is relatively small.[24,29−31] Furthermore, the net flux (i.e., combination of electromigration and diffusion) through the membrane is primarily contributed by the diffusion mechanism.[32] We can then integrate eq 4 to obtain the ion flux

$$J_i = K_{f,i}\mathcal{L}_{m,i}\Delta c_i \quad (7)$$

where $\mathcal{L}_{m,i}$ is the transmembrane mass transfer coefficient and Δc_i denotes the difference in the ion concentration across the

https://doi.org/10.1021/acs.est.2c09772
Environ. Sci. Technol. 2023, 57, 3930−3939

membrane. Note that $\mathcal{L}_{m,i}$ is related to D_i and membrane thickness, L_m

$$\mathcal{L}_{m,i} = \frac{D_i}{L_m} \tag{8}$$

To further simplify eq 7, we introduce the GCE model.[33−35] In brief, inside the membrane, the concentration of co-ions is orders of magnitude smaller than that of counter-ions. It has been demonstrated that the overall salt flux is controlled by the species with less permeability (i.e., co-ions).[20,21,23,32] Based on the GCE model, we can arrive at the following equation

$$J_s = K_{f,co}\mathcal{L}_{m,co}K_{co}\Delta c_{s,b} \tag{9}$$

where J_s is the salt flux, $K_{f,co}$ is the frictional factor of co-ions, $\mathcal{L}_{m,co}$ is the transmembrane mass transfer coefficient of co-ions, K_{co} is the partitioning coefficient of co-ions, and $\Delta c_{s,b}$ is the salt concentration difference between the feed and permeate bulk solutions. Based on eq 9, the salt permeability, B_{GCE}, can be obtained as

$$B_{GCE} = K_{f,co}\mathcal{L}_{m,co}K_{co} \tag{10}$$

Extracting Co-ion Partitioning from Salt Partitioning. Current continuum models consider three partitioning mechanisms of salt ions in RO and nanofiltration membranes: Donnan effect, steric exclusion, and dielectric exclusion.[7,28,36] The latter two, however, are not independent of each other as they are both related to pore size and ion size.[37−39] Herein, to simplify the complex partitioning phenomenon, we consider the classic Donnan effect and lump all the other partitioning mechanisms as non-Donnan effects. The former is due to the electrostatic interactions between ions and membrane, while the non-Donnan effects are primarily a function of the pore size and ion size (i.e., independent of salt concentration after accounting for the effects of water structure).[40] Hence, the partitioning of salt can be described by modifying the classic Donnan theory (assuming monovalent salt)

$$c_{ct,m} = c_{s,b}\Phi_{ct}\exp(-\Delta\varphi_D) \tag{11a}$$

$$c_{co,m} = c_{s,b}\Phi_{co}\exp(\Delta\varphi_D) \tag{11b}$$

$$c_{tot,m} = 2c_{s,b}\Phi\cosh(\Delta\varphi_D) \tag{11c}$$

$$c_{ct,m} - c_{co,m} + X = 0 \tag{11d}$$

Here, $c_{ct,m}$ and $c_{co,m}$ are the counter-ion and co-ion concentrations inside the membrane, respectively, Φ_{ct} and Φ_{co} are the counter-ion and co-ion non-Donnan partitioning coefficients, respectively, Φ is the non-Donnan partitioning coefficient (i.e., the geometric mean of Φ_{ct} and Φ_{co}, details in the Supporting Information), $\Delta\varphi_D$ is the dimensionless Donnan potential (i.e., Donnan potential divided by the thermal voltage, 0.0256 V at 25 °C), $c_{s,b}$ is the salt concentration in the solution outside the membrane, $c_{tot,m}$ is the total ion concentration inside the membrane (i.e., the sum of $c_{ct,m}$ and $c_{co,m}$), and X is the membrane charge density (a negative value).

To further simplify the analysis and experimental measurements, we assume that Φ_{ct} and Φ_{co} are equal. With this assumption and considering that Φ is the geometric mean of Φ_{ct} and Φ_{co}, we can obtain Φ from eq 11c, if the membrane charge that induces the Donnan effect is completely screened (i.e., $\Delta\varphi_D = 0$). Specifically, we perform QCM measurements (described in the Materials and Methods section) for the PA membrane with a solution of 1.2 M NaCl at a pH of 4.5. A high salt concentration screens the surface charge and pH 4.5, near the isoelectric point of the membrane,[18,41,42] eliminates the effect of electrostatic forces. Under these solution conditions, Φ can be determined following eq 11c once $c_{tot,m}$ is quantified via QCM measurements. Though the analytical approach is theoretically sound, the deswelling of the PA film at high salt concentrations would add uncertainty to the quantification of salt partitioning.[43]

For quantifying the co-ion partitioning coefficient, the Donnan potential, $\Delta\varphi_D$, must be determined. We calculate $\Delta\varphi_D$ from eq 11c using Φ (determined as described above), $c_{tot,m}$ (the total ion concentration inside the membrane determined from QCM measurements), and $c_{s,b}$ (salt concentration in the solution outside the membrane)

$$\Delta\varphi_D = -\cosh^{-1}\left(\frac{c_{tot,m}}{2c_{s,b}\Phi}\right) \tag{12}$$

Finally, the partitioning coefficients of the salt (total ions) and co-ions can be quantified using

$$K_{tot} = \Phi\cosh(\Delta\varphi_D) \tag{13a}$$

$$K_{co} = \Phi\exp(\Delta\varphi_D) \tag{13b}$$

where K_{tot} and K_{co} are the partitioning coefficients of total ions (i.e., salt) and co-ions, respectively. Note that because PA RO membranes are negatively charged, $\Delta\varphi_D$ in the above equations is negative. We also note that K_{co} is conceptually equivalent to the mobile salt partitioning coefficients in previous studies.[10,11]

MATERIALS AND METHODS

Materials and Chemicals. A stock solution of 5 M NaCl was prepared by dissolving sodium chloride in deionized (DI) water. The stock solution was used to adjust the salt concentration in the salt partitioning measurements and RO filtration experiments. The solution pH was adjusted by the addition of concentrated hydrochloric acid (HCl) or sodium hydroxyl (NaOH) solutions. All chemicals were ACS-grade (Fisher Scientific, Pittsburgh, PA). A commercial PA TFC RO membrane (SW30 XLE, Dow Chemical Company, Midland, MI) obtained as a flat sheet (purchased from Sterlitech Corporation) was used in our partitioning measurements and salt rejection experiments.

Membrane Sample Preparation. Before the partitioning measurements and salt rejection experiments, the as-received membrane was wetted by soaking in a solution of 25% v/v isopropanol in DI water for 30 min, followed by a thorough rinse with DI water three times. For the partitioning measurements, the PA active layer was isolated from RO membrane coupons onto 5 MHz QCM sensors (QSX 301 gold, Nanoscience Instruments, AZ). Specifically, the membrane coupon was first cut into a circular shape with an area of 0.78 cm^2, matching the size of the QCM sensor. Next, the polyester backing layer of the circular membrane coupon was peeled off with a tweezer, leaving a composite of the polysulfone support and PA layers. The composite membrane sample was then placed on the QCM sensor with the PA layer in contact with the sensor. Following this step, the composite membrane and the sensor were clamped between a glass plate and a cubic block with a cylindrical cutout (Figure S1). We

https://doi.org/10.1021/acs.est.2c09772
Environ. Sci. Technol. 2023, 57, 3930−3939

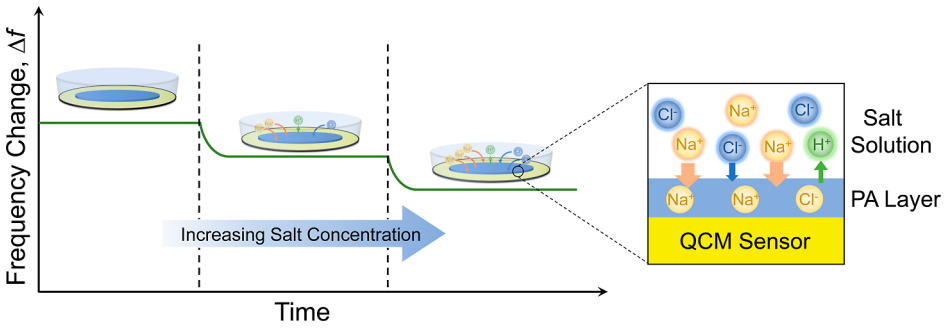

Figure 1. Schematic illustration of the QCM detecting the frequency change as the PA layer is exposed to increasing salt solution concentrations. The PA layer is coated onto the QCM sensor before mounting in the flow-by Q-sense module. The PA-coated sensor is equilibrated with DI water adjusted to the target pH overnight and then exposed to salt solutions with varying concentrations. The frequency decreases with increasing salt concentration as an increased mass of salt ions partition into the PA layer. At the interface between the PA layer and salt solution, salt ions adsorb to the membrane. Because of the negative charge of the PA membrane, more cations partition into the membrane as compared to anions.

note that the cylindrical hole matched the membrane composite before being clamped together. Last, dimethylformamide (DMF) was added inside the hole to dissolve the polysulfone layer, leaving the PA layer on the QCM sensor. To ensure the complete removal of the polysulfone, the DMF solution inside the hole was replaced five times. Before use, the QCM sensor coated with the PA layer was air-dried overnight in a hood.

Salt Partitioning Measurements with QCM. A QCM-D (Biolin Scientific, Sweden) was used to quantify the areal mass of the coated PA layer on the QCM sensor (m_{AL}) and the amount of partitioned salt into the PA layer (m_{salt}). A peristaltic pump (Ismatec, IDEX Corporation, IL) was used to provide influent flow to the Q-sense flow chamber where the PA-coated sensor was mounted beforehand. All tests were performed with a flow rate of 30 μL min^{-1} in a temperature-controlled (22 °C) environment.

To determine the areal mass of the coated PA layer, m_{AL}, we ran QCM tests with the sensors before and after they were coated with the PA layer in air. The frequency change (Δf) detected by QCM is related to the mass change (Δm) based on the Sauerbrey equation[44]

$$\Delta m = -C\frac{\Delta f}{n} \tag{14}$$

where n is the overtone number (n = 5 in this study) and C is the crystal constant (17.7 ng Hz^{-1} cm^{-2} for a 5 MHz QCM). The thickness of the PA layer (δ) is then obtained by dividing m_{AL} by the density of the PA layer (1.24 g cm^{-3}).[45−47] For different sets of experiments, δ was determined to be relatively stable (~100 nm, see the Supporting Information, Table S1).

Before each partitioning test, the sensor coated with the PA layer was mounted to the Q-sense flow chamber. To ensure full hydration of the PA layer, DI water, adjusted to the desired pH, continuously flowed through the chamber for 6 h. Then, a solution with the target pH and salt concentration was passed through the QCM flow chamber. Three solution pH values (i.e., 4.5, 6.0, and 10.2) were tested. For each solution pH, the salt (NaCl) concentration increased gradually as follows: 100, 200, 400, 600, and 800 mM (Figure 1). The coated sensor was exposed to the salt concentration until the frequency became stable with time. A typical frequency profile is shown in the Supporting Information (Figure S2). An uncoated sensor was also tested with the same solutions as a control to account for the changes in viscosity and density in the solutions.[19,48] The mass of the partitioned salt (m_{salt}) was determined from the frequency change recorded by the QCM after subtracting the frequency change detected by the uncoated sensors. This mass change (m_{salt}) was used to calculate the concentration of the salt partitioned into the membrane ($c_{s,p}$) as described elsewhere[10,11]

$$\Delta m = \delta(c_{s,v}f_v MW_v + c_{s,p}(1 - f_v)MW_p) \tag{15}$$

where δ is the membrane thickness, $c_{s,v}$ is the salt concentration in the PA membrane voids, f_v is the void fraction (f_v = 0.3),[49] and MW_v and MW_p are the molecular weights of the salt in the voids and in the membrane, respectively. Given that the voids in the rough, nodule-like PA active layer surface of RO membranes are tens of nanometers in size,[49] the salt concentration inside the voids ($c_{s,v}$) is the same as that in the bulk solution (i.e., no salt exclusion between bulk solution and voids). It is further assumed that MW_v is the molecular weight of the unhydrated NaCl, while MW_p is the hydrated molecular weight. The assumption might be valid considering that the PA film is not rigid and can accommodate the hydrated water molecules without displacing pre-existing water from the film, based on the work conducted by Coronell et al.[10,11] Additionally, MW_p is calculated from[10,11]

$$MW_p = MW_{unhydrated} + n_p MW_{water} \tag{16}$$

where $MW_{unhydrated}$ is the unhydrated molecular weight, n_p is the hydration number, and MW_{water} is the molecular weight of water. Previous studies determined that n_p = 12.3 for NaCl (i.e., assumed to be the same as in bulk solution).[11] The precise quantification of n_p is challenging and out of the scope of our study. Needless to mention, it will not change the trends presented in our study.

Once $c_{s,p}$ is obtained, the partitioning coefficient of salt (total ion), K_{tot}, can be determined from

$$K_{tot} = \frac{c_{s,p}}{2c_{s,b}} \tag{17}$$

RO Setup and Salt Rejection Measurements. The RO experiments were performed on a bench-scale cross-flow system. The system has a rectangular plate-and-frame feed flow channel with a length, width, and height of 7.7, 2.6, and 0.3 cm, respectively. Before adding salt to the feed, the membrane coupon was compacted at the target pressure for at least 6 h. Aliquots of NaCl stock solution were then added to the feed tank to reach the specified feed salt concentration. The

https://doi.org/10.1021/acs.est.2c09772
Environ. Sci. Technol. 2023, 57, 3930−3939

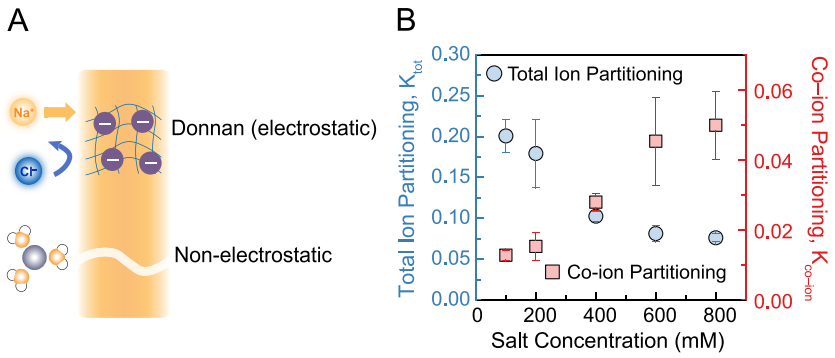

Figure 2. Characterization of salt and ion partitioning into the PA active layer of RO membranes. (A) Schematic illustration of the effect of membrane charge on salt partitioning. In addition to Donnan (electrostatic) partitioning, a nonelectrostatic partitioning, largely independent of charge, also takes place. (B) Total ion partitioning and co-ion partitioning coefficients as a function of salt (NaCl) concentration. The salt concentration varied from 100 to 800 mM NaCl, while the solution pH was fixed at 6.0. The flow rate to each Q-sense module of the QCM apparatus was 30 μL min^{-1}, and the solution temperature was set at 22 °C. Error bars indicate one standard deviation from duplicate experiments.

solution pH in the feed tank was adjusted by adding NaOH (1 M) or HCl (1 M). Three solution pH levels (i.e., 4.5, 6.0, and 10.2) were tested, with two salt concentrations (i.e., 200 and 350 mM NaCl) for each solution pH. After adding salt to the feed tank, the applied hydraulic pressure was adjusted to set the permeate water flux. Permeate samples were collected, and the conductivity of the samples was measured with a calibrated conductivity probe (Oakton CON 110, Oakton Instruments, IL). The conductivity was then converted to salt concentration using a predetermined calibration curve. During the experiments, the cross-flow velocity was fixed as 0.21 m s^{-1} and the temperature was maintained at 25 ± 0.5 °C. Duplicate experiments with two different membranes were conducted.

To evaluate the influence of feed salt concentration and feed solution pH, two performance metrics—salt rejection and salt permeability—were determined based on the RO experimental results

$$R_j = 1 - \frac{c_{perm}}{c_{feed}} \tag{18}$$

$$c_{mem} = c_{feed} \exp\left(\frac{J_w}{k}\right) \tag{19}$$

$$B_{exp} = \frac{c_{perm} J_w}{c_{mem} - c_{perm}} \tag{20}$$

Here, R_j is the observed salt rejection, B_{exp} is the membrane salt permeability (L m^{-2} h^{-1}), c_{feed} is the salt concentration in the feed, c_{mem} is the membrane salt concentration (i.e., at the interface between the membrane and feed solution), c_{perm} is the salt concentration in the permeate, J_w is the permeate water flux (L m^{-2} h^{-1}), and k is the mass transfer coefficient (L m^{-2} h^{-1}) in the concentration polarization layer. The latter (k = 74.9 L m^{-2} h^{-1}) was determined from the difference in the measured water fluxes before and after adding salt to the feed tank, as described elsewhere.[50,51]

RESULTS AND DISCUSSION

Comparison of Total Ion (Salt) Partitioning and Co-ion Partitioning. The overall partitioning of salt ions into the PA membrane involves electrostatic (i.e., Donnan) and nonelectrostatic mechanisms (Figure 2A). Due to the negative charge of the PA membrane, a Donnan potential is established at the interface between the solution and the membrane. Specifically, the electrical potential decreases at such an interface, resulting in a lower electrical potential inside the membrane relative to the electrical potential in the solution just outside the membrane (i.e., $\Delta\varphi_D$ is negative). Based on eqs 13a and 13b, we should expect that the partitioning coefficient of anions (i.e., K_{co}) would differ substantially from that of total ions (i.e., K_{tot}). Furthermore, the negative Donnan potential should lead to a smaller K_{co} than K_{tot}.

To quantify K_{tot}, we employed the QCM-D to measure the frequency change of the PA layer as it is exposed to solutions with known salt concentrations. Following eqs 13a–17, K_{tot} can be determined from the QCM measurements. As shown in Figure 2B, K_{tot} decreases as the feed salt concentration increases (the scatter plot is shown in the Supporting Information, Figure S3), in agreement with previous studies measuring the partitioning coefficients of salt by electrochemical impedance,[13,15] Rutherford backscattering spectroscopy,[16] and QCM-D.[10,11] The decreasing trend of K_{tot} is explicable in terms of the Donnan equilibrium. Increasing the salt concentration decreases the magnitude (i.e., absolute value) of the Donnan potential, resulting in a reduced K_{tot} (eq. 13a). This observation can also be explained by eq 13a: the diminished Donnan potential, stemming from the increase of salt concentration, reduces the partitioning of total ions.

The determination of K_{co} is not straightforward, requiring calculations via the modified Donnan theory (i.e., a combination of non-Donnan and Donnan mechanisms) as described above in the Theory Section. The overall non-Donnan partitioning coefficient (Φ) can be approached at a high salt concentration (i.e., 1200 mM in this study) and when the solution pH is near the isoelectric point of the membrane (i.e., pH = 4.5).[52] Following this method, K_{tot} was first determined under these solution conditions, where the Donnan potential can be assumed to be zero (i.e., $\Delta\varphi_D$ is zero in eq 13a). In this case, Φ is equivalent to K_{tot}, which is determined as 0.07 for our membrane (details are provided in the Supporting Information). Note that Φ does not depend on the salt concentration as we discussed in the Theory Section. Hence, the Donnan potential ($\Delta\varphi_D$) at each salt concentration can then be calculated with the known (measured) K_{tot} (determined from eq 17) and Φ. Following eq 13b, the co-ion partitioning coefficient, K_{co}, can be determined for a wide range of salt concentrations.

The calculated K_{co} values at various salt (NaCl) concentrations are shown in Figure 2B. The magnitude of K_{co} is about

https://doi.org/10.1021/acs.est.2c09772
Environ. Sci. Technol. 2023, 57, 3930−3939

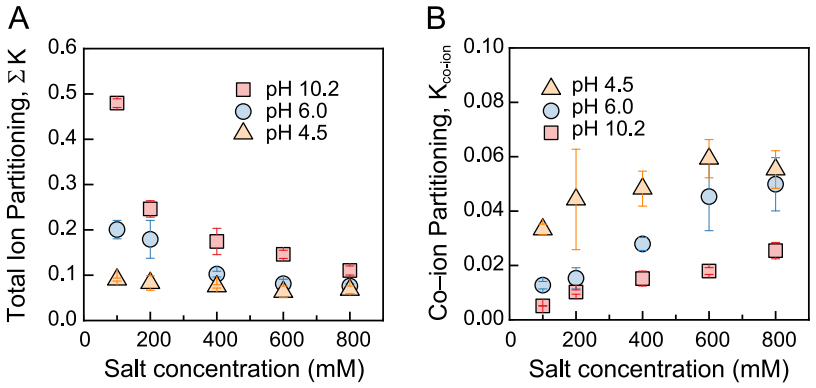

Figure 3. Effect of solution pH and salt concentration on partitioning coefficients. (A) Total ion partitioning coefficient and (B) co-ion partitioning coefficient as a function of salt (NaCl) concentration at various solution pHs: 4.5, 6.0, and 10.2. Before the QCM test, two PA layer-coated sensors in parallel were exposed to water with adjusted pH overnight. Then, salt concentration was gradually increased from 100 to 800 mM while the change in frequency was recorded. The flow rate to each Q-sense module was 30 μL min^{-1}, and the system temperature was set at 22 °C. Error bars indicate one standard deviation from duplicate experiments.

1 order of magnitude smaller than K_{tot} due to the negative charge, and hence the negative Donnan potential, of the PA membrane. In addition, K_{co} increases with increasing salt concentration, in marked contrast to the trend of K_{tot}. For example, as the salt concentration increases from 100 to 800 mM, K_{tot} decreases from 0.20 to 0.08, while K_{co} increases from 0.013 to 0.050. The dependence of K_{co} on salt concentration is governed by the Donnan effect. The diminished Donnan potential (i.e., less negative value) at higher salt concentrations leads to a lessened ability of the membrane to repel negatively charged co-ions. As a result, more co-ions partition into the membrane when exposed to higher salt concentrations.

The classic SD model describes salt permeability as the product of the salt partitioning coefficient and diffusion coefficient of salt within the membrane normalized by the membrane thickness. In addition, it has been reported in numerous studies that salt permeability increases as the salt concentration increases.[5,6,53] By comparing the trends of K_{co} and K_{tot} as a function of salt concentration shown in Figure 2B, we suggest that the salt permeability depends on K_{co}. In the following sections, the relationship between K_{co} and salt permeability will be thoroughly analyzed and discussed.

Total Ion Partitioning and Co-ion Partitioning Vary with Solution pH. As discussed in the previous subsection, the behavior of K_{tot} and K_{co} can be explained by the Donnan effect. The Donnan effect is a function of the membrane charge density as it determines the magnitude of the Donnan potential. In this subsection, we evaluate the dependence of K_{tot} and K_{co} on membrane charge. The charge of the membrane PA layer is a function of solution pH, resulting from the ionization of membrane carboxyl and amine groups.[17,41,54] Increasing the solution pH results in deprotonation of the carboxyl groups and hence an increase in the membrane charge density, and vice versa. The volumetric membrane charge density has been determined to be as high as 500 mM at pH > 10 and to be close to zero as the solution pH approaches 4.[18,19] Therefore, we tune the membrane charge by adjusting the solution pH. Specifically, we evaluate the partitioning coefficients at three solution pHs: 4.5, 6.0, and 10.2.

The magnitude of K_{tot} decreases when lowering the solution pH (Figure 3A); the corresponding scatter plot is shown in Figure S4A. Inside the negatively charged membrane, the amount of ion species is dominated by the counter-ions. As the Donnan potential decreases with the reduced membrane charge at lower solution pH, the capacity of the membrane to take up counter-ions decreases. Hence, K_{tot} decreases as the solution pH changes from alkaline to acidic. In addition, the dependence of K_{tot} on salt concentration becomes weaker as the solution pH decreases. On the other hand, at pH 10.2, carboxyl groups fully dissociate, rendering a large membrane charge. When the highly charged membrane is in contact with a low salt concentration solution, a large Donnan potential is established, resulting in an appreciable K_{tot}. However, the Donnan potential approaches zero as the salt concentration exceeds a certain value due to charge screening, significantly reducing K_{tot} (eq 13a). Therefore, K_{tot} changes drastically with salt concentration at alkaline pH, in comparison to acidic pH conditions.

The dependence of K_{co} on solution pH is in marked contrast to that of K_{tot}. As shown in Figure 3B (the corresponding scatter plot is shown in Figure S4B), the magnitude of K_{co} increases as the solution pH decreases, which is attributable to the reduced membrane charge. At the interface between the salt solution and the membrane, the established Donnan potential repels the co-ions and hinders their partitioning into the membrane. This co-ion repelling effect is prominent when the membrane carboxyl groups are fully dissociated in very alkaline conditions (i.e., pH 10.2), thus inhibiting the partitioning of co-ions. As the solution pH approaches the isoelectric point, the membrane charge drastically decreases, leading to increased K_{co}. Regardless of the solution pH, K_{co} in general increases with salt concentration, as we have shown before in Figure 2B. We also note that decreasing the solution pH weakens the dependence of K_{co} on salt concentration due to the lessened Donnan effect in low-pH solutions. Similar observations have been revealed by a previous study where the partitioning of the mobile salt increases as the solution pH decreases.[10]

As discussed in the previous subsection, the dependence of K_{co} on salt concentration is in line with that of salt permeability reported by several studies[5,6,53]—both parameters increase with increasing salt concentration. This trend of K_{co} is consistently observed even when the solution pH is changed over a wide range. In addition, the magnitude of K_{co} increases when decreasing the solution pH. To verify the relationship

https://doi.org/10.1021/acs.est.2c09772
Environ. Sci. Technol. 2023, 57, 3930−3939

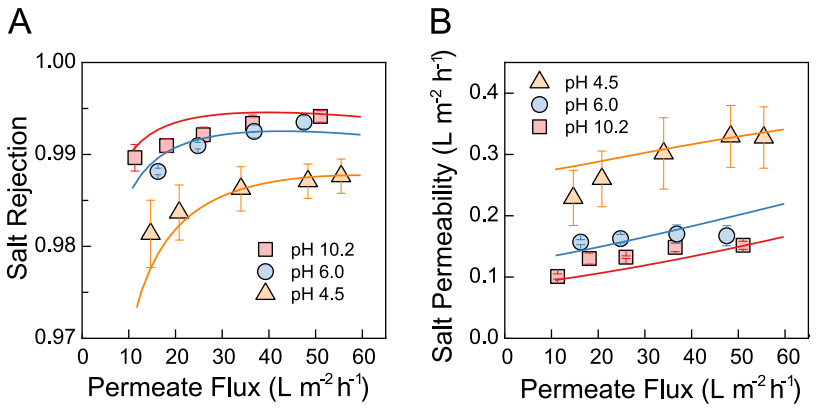

Figure 4. RO performance (salt rejection and salt permeability) determined at various solution pHs. (A) Salt rejection and (B) salt permeability as a function of permeate water flux at three solution pHs: 4.5, 6.0, and 10.2. The experimental data were collected with a customized cross-flow RO system operating at a cross-flow velocity of 0.21 m s^{-1}, a temperature of 22 °C, and a feed salt concentration of 200 mM. The open symbols represent the experimental data, while the solid lines represent the SF model predictions. Error bars indicate one standard deviation from duplicate experiments.

between salt permeability and K_{co} under differing solution pH, we performed RO experiments at different feed solution pHs to determine salt permeability from the measured salt rejection.

Salt Rejection and Permeability Vary with Solution pH. RO experiments at varying feed solution pH were conducted to evaluate the influence of pH on salt rejection and salt permeability. Similar to the measurements of partitioning coefficients, three solution pH values were tested in the cross-flow RO system. For each pH, the RO experiments were conducted at varying feed salt concentrations and applied hydraulic pressures. Salt rejection and salt permeability as a function of permeate water flux and feed solution pH for a fixed feed concentration (i.e., 200 mM) are presented in Figure 4 (the corresponding scatter plots are in Figure S5). Additional data on salt rejection and salt permeability for different feed concentrations are provided in the Supporting Information (Figure S6). Salt rejection is enhanced by increasing the permeate water flux due to the dilution of the permeate solution (often called the "dilution effect") (Figure 4A). In addition, a higher salt rejection is observed with an increased solution pH. Specifically, the salt rejection dramatically increases as the solution pH increases from 4.5 to 6.0, while the extent of salt rejection enhancement is less prominent as the solution pH is further increased to 10.2. Accordingly, salt permeability, inversely related to the resistance of the membrane to salt transport, decreases as the solution pH switches from acidic to alkaline (Figure 4B). Similar to the dependence of salt rejection on solution pH, the difference between the salt permeabilities at pH 4.5 and pH 6.0 is greater than that between pH 6.0 and pH 10.2.

The SF model was employed to theoretically calculate the salt rejection and salt permeability as a function of permeate water fluxes for each solution pH. The SF model was described in the Theory Section as well as in our recent publications.[5] The modeling results predict the experimental data of salt rejection and salt permeability at the various experimental conditions very well (Figure 4, solid lines), highlighting the reliability and robustness of the SF model. The parameters used in the model are summarized in Table S2. We note that the membrane charge density for each solution pH was obtained by fitting the experimental partitioning coefficients in Figure 3 to the SF model (details in Figure S7). In addition, $K_{f,i}$ was determined to be 0.003 by fitting the RO experimental data to the SF model.

The effect of solution pH on salt rejection and salt permeability is attributed to the dependence of membrane charge on solution pH. Membrane charge, resulting from the deprotonation of carboxyl groups, is a function of solution pH, varying from near zero at pH ∼4 to 500 mM at pH > 10.[19] As a result, when the solution pH increases from 4.5 to 10.2, the magnitude of the Donnan potential increases. As we have shown earlier, co-ion partitioning decreases when increasing the solution pH from 4.5 to 10.2, resulting from the enhanced magnitude of the Donnan potential (Figure 3B). Therefore, the trend of salt permeability matches that of the partitioning coefficient of co-ions, suggesting that the salt permeability is determined by co-ion partitioning.

Co-ion Partitioning, Not Salt Partitioning, Governs Salt Permeability. To illustrate the relationship between salt permeability and the co-ion partitioning coefficient, we presented an analytical equation derived from the rigorous SF model to quantify the dependence of salt permeability on the partitioning coefficient of co-ions (eq 10). Based on the K_{co} values derived from QCM measurements (Figure 3B), we can theoretically calculate the salt permeability following eq 10. However, we need to quantify the transmembrane mass transfer coefficient and the frictional factor of co-ions before applying the equation. The diffusion-based mass transfer coefficient, $\mathcal{L}_{m,co}$, depends on the bulk diffusion coefficient of the ions, the effective porosity, and the thickness of the membrane (details of estimating $\mathcal{L}_{m,co}$ are presented in the Supporting Information), while the frictional factor, $K_{f,co}$, depends on the frictions between the co-ions and the membrane as well as between the co-ions and water (eq 5). The frictional factor ranges from zero to 1, with 1 indicating no friction and zero meaning infinitely large friction between the ions and membrane.

Based on eq 10, the salt permeability, B_{GCE}, can be determined as a function of K_{co} as the latter has been experimentally determined via QCM measurements. Since we have already quantified K_{co} at varying feed salt concentrations and solution pH, we can now plot B_{GCE} as a function of salt concentration for the three solution pH values (data points in Figure 5, with the corresponding scatter plot shown in Figure

https://doi.org/10.1021/acs.est.2c09772
Environ. Sci. Technol. 2023, 57, 3930−3939

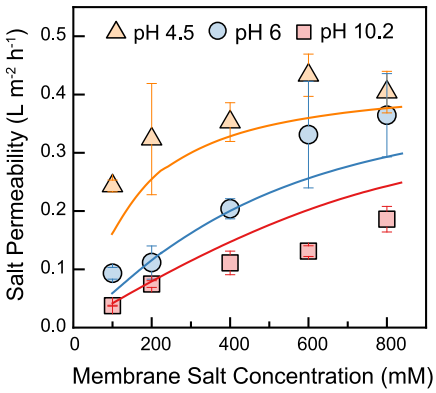

Figure 5. Comparison of salt permeabilities obtained from the SF model (lines), which was validated based on RO experiments, and those obtained with the GCE model based on the experimentally determined co-ion partitioning coefficient (symbols). The RO experimental data were collected on a customized cross-flow system with a cross-flow velocity of 0.21 m s^{-1} and a temperature of 22 °C. The feed salt concentration and solution pH were varied in the RO experiments. The co-ion partitioning coefficients in Figure 3B were used to calculate the salt permeability following eq 10 with a mass transfer coefficient ($\mathcal{L}_{m,co}$) of 2436 L m^{-2} h^{-1} (0.677 mm s^{-1}). The other parameters used are provided in the Supporting Information.

S8). Furthermore, we do not differentiate the frictional factor for Na^+ and Cl^- (i.e., $K_{f,co}$ is equal to 0.003). We also present the salt permeabilities as a function of membrane surface salt concentration generated by the rigorous SF model (solid curves in Figure 5), which was validated by the RO experiments. To account for the effect of concentration polarization, the membrane surface salt concentrations were calculated following eq 19.

The results in Figure 5 show that the salt permeabilities based on the GCE model using the measured co-ion partitioning coefficients are in good agreement with the SF model. Notably, the GCE model, coupled with the modified Donnan theory, well captures the variation of salt permeability with salt concentration and solution pH. Overall, the results indicate the significance of K_{co} in governing the salt permeability of RO.

IMPLICATIONS

The salt permeability of RO membranes is a critical metric for evaluating RO performance. However, a mechanistic understanding of salt permeability in RO is lacking. For example, recent studies revealed that salt permeability increases at higher salt concentrations, in marked contrast to the classic SD model that assumes a constant salt permeability for RO membranes. Within the general framework of the SD model, the dependence of salt permeability on salt concentration has been ascribed to the variation of the salt partitioning coefficient with salt concentration. However, salt partitioning has been demonstrated to decrease with increasing salt concentration, in contrast to the predictions by the SD model.

Our findings emphasize the dependence of salt permeability on solution chemistry (i.e., salt concentration and solution pH). It is therefore necessary to employ the same operating and solution conditions (i.e., salt concentration and solution pH) when evaluating the performance of different RO membranes. Importantly, both experiments and the theory presented in this study demonstrate that salt permeability is governed by the partitioning of co-ions. Specifically, the good agreement between the GCE model and RO experimental results supports our conclusion that partitioning and diffusion of co-ions, not salt (total ions), govern salt transport behavior in RO. Our study advances the fundamental understanding of salt permeation through RO membranes, serving as an important tool for developing better protocols for membrane performance characterization.

Our study resolves the controversial trends between the salt partitioning obtained from various analytical techniques (e.g., QCM) and salt permeability observed in RO experiments. The highlighted significance of co-ion partitioning and membrane charge has important implications for RO membrane fabrication and performance optimization. For example, our findings suggest that enhancing membrane charge density would improve salt rejection. Such improvement is particularly prominent when treating feed waters with low salt concentrations (e.g., wastewater effluent or brackish water).

ASSOCIATED CONTENT

Supporting Information

The Supporting Information is available free of charge at https://pubs.acs.org/doi/10.1021/acs.est.2c09772.

Overall non-Donnan partitioning coefficient; transmembrane mass transfer coefficient; setup for coating polyamide active layer on QCM sensors; representative frequency change of a polyamide-coated QCM sensor exposed to NaCl solutions; scatter plot of total ion partitioning and co-ion partitioning coefficients as a function of salt (NaCl) concentration; effect of solution pH and salt concentration on partitioning coefficients; RO performance (salt rejection and salt permeability) determined at various solution pHs; RO experimental results of salt rejection and salt permeability as a function of permeate water flux at varying solution pH and salt concentrations; comparison of the solution–friction model predictions with experimentally determined partitioning coefficients; comparison of salt permeabilities obtained from the SF model and those obtained with the GCE model based on the experimentally determined co-ion partitioning coefficient; thickness measurements of the coated polyamide layer; and parameters used in the salt and water RO transport model (PDF)

AUTHOR INFORMATION

Corresponding Author

Menachem Elimelech − *Department of Chemical and Environmental Engineering, Yale University, New Haven, Connecticut 06520-8286, United States;* orcid.org/0000-0003-4186-1563; Phone: +1 (203) 432-2789; Email: menachem.elimelech@yale.edu

Authors

Li Wang − *Department of Chemical and Environmental Engineering, Yale University, New Haven, Connecticut 06520-8286, United States;* orcid.org/0000-0002-5542-6696

Tianchi Cao − *Department of Chemical and Environmental Engineering, Yale University, New Haven, Connecticut 06520-8286, United States*

https://doi.org/10.1021/acs.est.2c09772
Environ. Sci. Technol. 2023, 57, 3930−3939

Kevin E. Pataroque − *Department of Chemical and Environmental Engineering, Yale University, New Haven, Connecticut 06520-8286, United States*
Masashi Kaneda − *Department of Chemical and Environmental Engineering, Yale University, New Haven, Connecticut 06520-8286, United States*
P. Maarten Biesheuvel − *European Centre of Excellence for Sustainable Water Technology, Wetsus, Leeuwarden 8911 MA, The Netherlands;* orcid.org/0000-0002-5468-559X

Complete contact information is available at: https://pubs.acs.org/10.1021/acs.est.2c09772

Notes

The authors declare no competing financial interest.

■ ACKNOWLEDGMENTS

This work was supported by the CENT, an Energy Frontier Research Center funded by the U.S. Department of Energy, Office of Science, Basic Energy Sciences, under award no. DE-SC0019112, and by the U.S. National Science Foundation (NSF) and U.S.-Israel Binational Science Foundation (BSF) under Award CBET-2110138.

■ REFERENCES

(1) Baker, R. W. *Membrane Technology and Applications*, 3rd ed.; Wiley, 2012; pp 207-251.
(2) Lu, X. L.; Elimelech, M. Fabrication of desalination membranes by interfacial polymerization: history, current efforts, and future directions. *Chem. Soc. Rev.* **2021**, *50*, 6290−6307.
(3) Wijmans, J. G.; Baker, R. W. The Solution-Diffusion Model - a Review. *J. Membr. Sci.* **1995**, *107*, 1−21.
(4) Paul, D. R. Reformulation of the solution-diffusion theory of reverse osmosis. *J. Membr. Sci.* **2004**, *241*, 371−386.
(5) Wang, L.; Cao, T. C.; Dykstra, J. E.; Porada, S.; Biesheuvel, P. M.; Elimelech, M. Salt and Water Transport in Reverse Osmosis Membranes: Beyond the Solution-Diffusion Model. *Environ. Sci. Technol.* **2021**, *55*, 16665−16675.
(6) Jang, E. S.; Mickols, W.; Sujanani, R.; Helenic, A.; Dilenschneider, T. J.; Kamcev, J.; Paul, D. R.; Freeman, B. D. Influence of concentration polarization and thermodynamic non-ideality on salt transport in reverse osmosis membranes. *J. Membr. Sci.* **2019**, *572*, 668−675.
(7) Kezia, K.; Lee, J.; Ogieglo, W.; Hill, A.; Benes, N. E.; Kentish, S. E. The transport of hydronium and hydroxide ions through reverse osmosis membranes. *J. Membr. Sci.* **2014**, *459*, 197−206.
(8) Geise, G. M.; Park, H. B.; Sagle, A. C.; Freeman, B. D.; McGrath, J. E. Water permeability and water/salt selectivity tradeoff in polymers for desalination. *J. Membr. Sci.* **2011**, *369*, 130−138.
(9) Geise, G. M.; Paul, D. R.; Freeman, B. D. Fundamental water and salt transport properties of polymeric materials. *Prog. Polym. Sci.* **2014**, *39*, 1−42.
(10) Wang, J. B.; Armstrong, M. D.; Grzebyk, K.; Vickers, R.; Coronell, O. Effect of Feed Water pH on the Partitioning of Alkali Metal Salts from Aqueous Phase into the Polyamide Active Layers of Reverse Osmosis Membranes. *Environ. Sci. Technol.* **2021**, *55*, 3250−3259.
(11) Wang, J. B.; Kingsbury, R. S.; Perry, L. A.; Coronell, O. Partitioning of Alkali Metal Salts and Boric Acid from Aqueous Phase into the Polyamide Active Layers of Reverse Osmosis Membranes. *Environ. Sci. Technol.* **2017**, *51*, 2295−2303.
(12) Coronell, O.; Mi, B.; Mariñas, B. J.; Cahill, D. G. Modeling the Effect of Charge Density in the Active Layers of Reverse Osmosis and Nanofiltration Membranes on the Rejection of Arsenic(III) and Potassium Iodide. *Environ. Sci. Technol.* **2013**, *47*, 420−428.
(13) Bason, S.; Oren, Y.; Freger, V. Characterization of ion transport in thin films using electrochemical impedance spectroscopy II: Examination of the polyamide layer of RO membranes. *J. Membr. Sci.* **2007**, *302*, 10−19.
(14) Freger, V.; Bason, S. Characterization of ion transport in thin films using electrochemical impedance spectroscopy. I. Principles and theory. *J. Membr. Sci.* **2007**, *302*, 1−9.
(15) Shaffer, D. L.; Feldman, K. E.; Chan, E. P.; Stafford, G. R.; Stafford, C. M. Characterizing salt permeability in polyamide desalination membranes using electrochemical impedance spectroscopy. *J. Membr. Sci.* **2019**, *583*, 248−257.
(16) Zhang, X. J.; Cahill, D. G.; Coronell, O.; Mariñas, B. J. Partitioning of salt ions in FT30 reverse osmosis membranes. *Appl. Phys. Lett.* **2007**, *91*, 181904.
(17) Chen, D.; Werber, J. R.; Zhao, X.; Elimelech, M. A facile method to quantify the carboxyl group areal density in the active layer of polyamide thin-film composite membranes. *J. Membr. Sci.* **2017**, *534*, 100−108.
(18) Coronell, O.; Mariñas, B. J.; Zhang, X. J.; Cahill, D. G. Quantification of functional groups and modeling of their ionization behavior in the active layer of FT30 reverse osmosis membrane. *Environ. Sci. Technol.* **2008**, *42*, 5260−5266.
(19) Perry, L. A.; Coronell, O. Reliable, bench-top measurements of charge density in the active layers of thin-film composite and nanocomposite membranes using quartz crystal microbalance technology. *J. Membr. Sci.* **2013**, *429*, 23−33.
(20) Yaroshchuk, A.; Martínez-Lladó, X.; Llenas, L.; Rovira, M.; de Pablo, J. Solution-diffusion-film model for the description of pressure-driven trans-membrane transfer of electrolyte mixtures: One dominant salt and trace ions. *J. Membr. Sci.* **2011**, *368*, 192−201.
(21) Pages, N.; Yaroshchuk, A.; Gibert, O.; Cortina, J. L. Rejection of trace ionic solutes in nanofiltration: Influence of aqueous phase composition. *Chem. Eng. Sci.* **2013**, *104*, 1107−1115.
(22) Reig, M.; Licon, E.; Gibert, O.; Yaroshchuk, A.; Cortina, J. L. Rejection of ammonium and nitrate from sodium chloride solutions by nanofiltration: Effect of dominant-salt concentration on the trace-ion rejection. *Chem. Eng. J.* **2016**, *303*, 401−408.
(23) Yaroshchuk, A.; Bruening, M. L.; Licón Bernal, E. E. Solution-Diffusion−Electro-Migration model and its uses for analysis of nanofiltration, pressure-retarded osmosis and forward osmosis in multi-ionic solutions. *J. Membr. Sci.* **2013**, *447*, 463−476.
(24) Biesheuvel, P. M.; Porada, S.; Elimelech, M.; Dykstra, J. E. Tutorial review of reverse osmosis and electrodialysis. *J. Membr. Sci.* **2022**, *647*, 120221.
(25) Noordman, T. R.; Wesselingh, J. A. Transport of large molecules through membranes with narrow pores - The Maxwell-Stefan description combined with hydrodynamic theory. *J. Membr. Sci.* **2002**, *210*, 227−243.
(26) Mehta, G. D.; Morse, T. F.; Mason, E. A.; Daneshpajooh, M. H. Generalized Nernst-Planck and Stefan-Maxwell Equations for Membrane-Transport. *J. Chem. Phys.* **1976**, *64*, 3917−3923.
(27) Tedesco, M.; Hamelers, H. V. M.; Biesheuvel, P. M. Nernst-Planck transport theory for (reverse) electrodialysis: II. Effect of water transport through ion-exchange membranes. *J. Membr. Sci.* **2017**, *531*, 172−182.
(28) Oren, Y. S.; Biesheuvel, P. M. Theory of Ion and Water Transport in Reverse-Osmosis Membranes. *Phys. Rev. Appl.* **2018**, *9*, 024034.
(29) Zhang, L.; Hamelers, H. V. M.; Biesheuvel, P. M. Modeling permeate pH in RO membranes by the extended Donnan steric partitioning pore model. *J. Membr. Sci.* **2020**, *613*, 118511.
(30) Biesheuvel, P. M.; Porada, S.; Elimelech, M.; Dykstra, J. E. Tutorial review of Reverse Osmosis and Electrodialysis. *J. Membr. Sci.* **2022**, *647*, 120221.
(31) Kedem, O.; Freger, V. Determination of concentration-dependent transport coefficients in nanofiltration: Defining an optimal set of coefficients. *J. Membr. Sci.* **2008**, *310*, 586−593.
(32) Yaroshchuk, A.; Bruening, M. L. An analytical solution of the solution-diffusion-electromigration equations reproduces trends in ion rejections during nanofiltration of mixed electrolytes. *J. Membr. Sci.* **2017**, *523*, 361−372.

(33) Zhang, C.; Guo, Y.; Wang, C.; Li, S.; Curnick, O.; Amietszajew, T.; Bhagat, R. Papers A new design of experiment method for model parametrisation of lithium ion battery. *J. Energy Storage* **2022**, *50*, 104301.
(34) Starov, V. M.; Churaev, N. V. Separation of Electrolyte-Solutions by Reverse-Osmosis. *Adv. Colloid Interface* **1993**, *43*, 145−167.
(35) Lefebvre, X.; Palmeri, J. Nanofiltration theory: Good co-ion exclusion approximation for single salts. *J. Phys. Chem. B* **2005**, *109*, 5525−5540.
(36) Biesheuvel, P. M.; Zhang, L.; Gasquet, P.; Blankert, B.; Elimelech, M.; van der Meer, W. G. J. Ion Selectivity in Brackish Water Desalination by Reverse Osmosis: Theory, Measurements, and Implications. *Environ. Sci. Technol. Lett.* **2020**, *7*, 42−47.
(37) Fumagalli, L.; Esfandiar, A.; Fabregas, R.; Hu, S.; Ares, P.; Janardanan, A.; Yang, Q.; Radha, B.; Taniguchi, T.; Watanabe, K.; Gomila, G.; Novoselov, K. S.; Geim, A. K. Anomalously low dielectric constant of confined water. *Science* **2018**, *360*, 1339.
(38) Richards, L. A.; Schäfer, A. I.; Richards, B. S.; Corry, B. The Importance of Dehydration in Determining Ion Transport in Narrow Pores. *Small* **2012**, *8*, 1701−1709.
(39) Lu, C. H.; Hu, C. Z.; Ritt, C. L.; Hua, X.; Sun, J. Q.; Xia, H. L.; Liu, Y. Y.; Li, D. W.; Ma, B. W.; Elimelech, M.; Qu, J. H. In Situ Characterization of Dehydration during Ion Transport in Polymeric Nanochannels. *J. Am. Chem. Soc.* **2021**, *143*, 14242−14252.
(40) Yaroshchuk, A.; Bruening, M. L.; Zholkovskiy, E. Modelling nanofiltration of electrolyte solutions. *Adv. Colloid Interface* **2019**, *268*, 39−63.
(41) Mouhoumed, E. I.; Szymczyk, A.; Schafer, A.; Paugam, L.; La, Y. H. Physico-chemical characterization of polyamide NF/RO membranes: Insight from streaming current measurements. *J. Membr. Sci.* **2014**, *461*, 130−138.
(42) Jiang, Z. W.; Karan, S.; Livingston, A. G. Water Transport through Ultrathin Polyamide Nanofilms Used for Reverse Osmosis. *Adv. Mater.* **2018**, *30*, 1705973.
(43) Freger, V. Swelling and Morphology of the Skin Layer of Polyamide Composite Membranes: An Atomic Force Microscopy Study. *Environ. Sci. Technol.* **2004**, *38*, 3168−3175.
(44) Sauerbrey, G. Verwendung Von Schwingquarzen Zur Wagung Dunner Schichten Und Zur Mikrowagung. *Z. Phys.* **1959**, *155*, 206−222.
(45) Lin, L.; Feng, C. C.; Lopez, R.; Coronell, O. Identifying facile and accurate methods to measure the thickness of the active layers of thin-film composite membranes - A comparison of seven characterization techniques. *J. Membr. Sci.* **2016**, *498*, 167−179.
(46) Kolev, V.; Freger, V. Hydration, porosity and water dynamics in the polyamide layer of reverse osmosis membranes: A molecular dynamics study. *Polymer* **2014**, *55*, 1420−1426.
(47) Zhang, X. J.; Cahill, D. G.; Coronell, O.; Marinas, B. J. Absorption of water in the active layer of reverse osmosis membranes. *J. Membr. Sci.* **2009**, *331*, 143−151.
(48) O'Sullivan, C. K.; Guilbault, G. G. Commercial quartz crystal microbalances - theory and applications. *Biosens. Bioelectron.* **1999**, *14*, 663−670.
(49) Lin, L.; Lopez, R.; Ramon, G. Z.; Coronell, O. Investigating the void structure of the polyamide active layers of thin-film composite membranes. *J. Membr. Sci.* **2016**, *497*, 365−376.
(50) Sutzkover, I.; Hasson, D.; Semiat, R. Simple technique for measuring the concentration polarization level in a reverse osmosis system. *Desalination* **2000**, *131*, 117−127.
(51) Nghiem, L. D.; Schäfer, A. I.; Elimelech, M. Removal of natural hormones by nanofiltration membranes: Measurement, modeling, and mechanisms. *Environ. Sci. Technol.* **2004**, *38*, 1888−1896.
(52) Hurwitz, G.; Guillen, G. R.; Hoek, E. M. V. Probing polyamide membrane surface charge, zeta potential, wettability, and hydrophilicity with contact angle measurements. *J. Membr. Sci.* **2010**, *349*, 349−357.
(53) Freger, V. Ion partitioning and permeation in charged low-T* membranes. *Adv. Colloid Interface* **2020**, *277*, 102107.
(54) Coronell, O.; González, M. I.; Mariñas, B. J.; Cahill, D. G. Ionization Behavior, Stoichiometry of Association, and Accessibility of Functional Groups in the Active Layers of Reverse Osmosis and Nanofiltration Membranes. *Environ. Sci. Technol.* **2010**, *44*, 6808−6814.

https://doi.org/10.1021/acs.est.2c09772
Environ. Sci. Technol. 2023, 57, 3930−3939